Supporting Information for

A Novel Framework for Calibration and Evaluation of Hydrological Models in Dynamic Catchments

Tian Lan[1,2,3], Xiao Wang[4*], Hongbo Zhang[1,2,3], Xinghui Gong[1,2,3], Xue Xie[5], Yongqin David Chen[6], Chong-Yu Xu[7]

[1]School of Water and Environment, Chang'an University, Xi'an 710054, China.
[2]Key Laboratory of Subsurface Hydrology and Ecological Effects in Arid Region of the Ministry of Education, Chang'an University, Xi'an 710054, China.
[3]Key Laboratory of Eco-Hydrology and Water Security in Arid and Semi-Arid Regions of Ministry of Water Resources, Chang'an University, Xi'an 710054, China.
[4]State Key Laboratory of Water Resources Engineering and Management, Wuhan University, Wuhan, China
[5]Center for Water Resources and Environment, and Guangdong Key Laboratory of Marine Civil Engineering, School of Civil Engineering, Sun Yat-sen University, Guangzhou 510275, China
[6]School of Humanities and Social Science, The Chinese University of Hong Kong, Shenzhen 518172, China.
[7]Department of Geosciences, University of Oslo, P.O. Box 1047 Blindern, 0316 Oslo, Norway.

Correspondence to: Xiao Wang (xiao_wang@whu.edu.cn)

Contents of this file

Introduction

This supporting information includes five sections that support the analysis. The *S1 Key parameters and metrics for the proposed framework* introduce the concept of model parameters and evaluation metrics used in this study. The *S2 Assistive techniques for the proposed framework* introduce the techniques used in this study. The *S3 Seasonal dynamic catchment characteristics* sections are used to support the *2.2 Seasonal dynamic catchment characteristics* section in the main manuscript. The *S4 Test results of the EDCC framework on the MOPEX dataset* is used to support the *4.1 Model performance* in the main manuscript. The *S5 State variables and fluxes assessment in the study cases* section is used to support the *4.2 State variables and fluxes* section in the main manuscript. The *S6 Correlation between model parameters* is used to support the *5.1.1 Complex correlation between parameters* section in the main manuscript.

S1 Key parameters and metrics for proposed framework

Table S1. HYMOD model parameters, state variables and fluxes (Vrugt et al., 2003; Wagener et al., 2001)

Label	Property	Range	Description
H_{uz}	Parameter	10–1500 mm	Maximum height of the soil moisture accounting tank
B	Parameter	0–1.99 mm	Scaled distribution function shape
α	Parameter	0–0.99 mm	Quick or slow split
K_q	Parameter	0–0.99 mm	Quick-flow routing tanks' rate
K_s	Parameter	0–0.99 mm	Slow-flow routing tank's rate
XH_{uz}	State variable	mm	Upper-zone soil moisture tank state height
XC_{uz}	State variable	mm	Upper-zone soil moisture tank state contents
X_q	State variable	mm	Quick-flow tank state contents
X_s	State variable	mm	Slow-flow tank state contents
AE	Flux	mm d^{-1}	Actual evapotranspiration flux
OV	Flux	mm d^{-1}	Precipitation excess flux
Q_q	Flux	mm d^{-1}	Quick-flow flux
Q_s	Flux	mm d^{-1}	Slow-flow flux
Q_sim	Flux	mm d^{-1}	Total simulated streamflow flux

Table S2. Description of performance metrics.

No.	Metric	Description
1	NSE	Sensitive to peaks and discharge dynamic
2	LNSE	Emphasizing low flows with the log of discharge
3	RMSE	RMSE sensitive to flood peaks
4	MSE	MSE sensitive to high flow
5	MSEL	MSEL sensitive to low flow
6	MAE	MAE measuring the overall discharge
7	RMSE_Q5	RMSE in FDC Q5 very-high-segment volume
8	RMSE_Q20	RMSE in FDC between Q5 and Q20 high-segment volume
9	RMSE_Qmid	RMSE in FDC between Q20 and Q70 mid-segment volume
10	RMSE_Q70	RMSE in FDC between Q70 and Q95 low-segment volume
11	RMSE_Q95	RMSE in FDC Q95 very-low-segment volume

Note that the FDC is usually split into different segments to describe different flow characteristics of a catchment (Gupta et al., 2009; Cheng et al., 2012; Pfannerstill et al., 2014). The RMSE with quadratic character is usually used to evaluate poor model performance due to the strong sensitivity to extreme positive and negative error values.

S2 Assistive techniques for the proposed framework

S2.1 Hamon potential evapotranspiration equation

To fill in missing data and ensure data consistency, this study employs the Hamon potential evapotranspiration equation to calculate potential evapotranspiration. The Hamon-derived evaporation equation is as simple as possible. He only used two main input parameters, including the temperature and sunshine hours. The developed equation is applicable to both humid and dry climatic conditions(Mccabe et al., 2015). According to this method, the evaporation may be calculated as follows(Hamon, 1961; Morton, 1971):

$$E = B_1(D)^{B_2} 10^{\left(\frac{B_3 T_{\text{mean}}}{T_{\text{mean}+273}}\right)} \tag{1}$$

where D is the maximum sunshine duration ratio and T_{mean} is the mean air temperature. The value of D may be estimated using the equation given below. B_1, B_2, and B_3 are constants with typical values of 0.63, 2.0, and 7.5, respectively.

$$D = \frac{1}{90}\arccos\left(-\tan(\varnothing)\,.\tan 23.45°\sin\left(\frac{J-80}{365}\right)360°\right) \tag{2}$$

In this equation, *"ϕ"* is the latitude and J represents the Julian day (Ghumman et al., 2021).

S2.2 Maximal information coefficient (MIC)

The MIC, as proposed by Reshef et al. (2011), is a measurement approach that doesn't rely on the distributional assumptions of datasets. This method captures extensive mutual information between variables, whether they exhibit functional or non-functional relationships. In the case of functional relationships, the MIC algorithm provides a score similar to the coefficient of determination (R^2) of the datasets. We analyze the datasets using the SG-MIC algorithm (utilizing simulated annealing and genetic techniques) developed for optimal MIC calculation. Convergence of the SG-MIC is established based on Markov theory (Zhang et al., 2014).

S2.3 Principal component analysis (PCA)

PCA is a multivariate statistical procedure that reduces data redundancy and unveils embedded patterns. This algorithm employs orthogonal transformations to convert a set of potentially correlated variables into linearly uncorrelated vectors with lower dimensionality. These resulting vectors, referred to as Principal Components (PCs), are orthogonal because the eigenvectors of the covariance matrix are symmetric. The first PC captures the maximum possible variance (Frey and Pimentel, 1978; Wright et al., 2009; Fan et al., 2017; Wold et al., 1987).

S2.4 Fuzzy C-means clustering (FCM)

The FCM clustering approach is a widely used probabilistic-type clustering method originally proposed by Dunn (1973) and further improved by Bezdek et al. (1984). The FCM algorithm can be summarized as follows: First, initialize the membership function matrix μ_{ij} based on the selected value of m. Second, compute the cluster center z_j and the Euclidean distance d_{ij}. Finally, update the membership function μ_{ij} once the iteration has converged. The termination criterion for the FCM algorithm is a low relative change in the cluster center values. It's important to note that the FCM algorithm is sensitive to initial conditions (Hathaway and Bezdek, 2001).

S2.5 Shuffled Complex Evolution approach (SCE-UA)

The shuffled complex evolution approach (SCE-UA), as an effective global optimization method, is a commonly used algorithm, because it is open source and was the first algorithm aimed specifically at calibrating hydrological models (Khakbaz and Kazeminezhad, 2012; Eckhardt and Arnold, 2001; Duan et al., 1994; Sorooshian et al., 2010). The technical details of the SCE-UA can be shown in the flowchart (see Fig. S1) (Duan et al., 1994). In the SCE-UA, the upper limit of the objective function evaluation is set to 10,000 times. All other settings of the SCE-UA technique are the default.

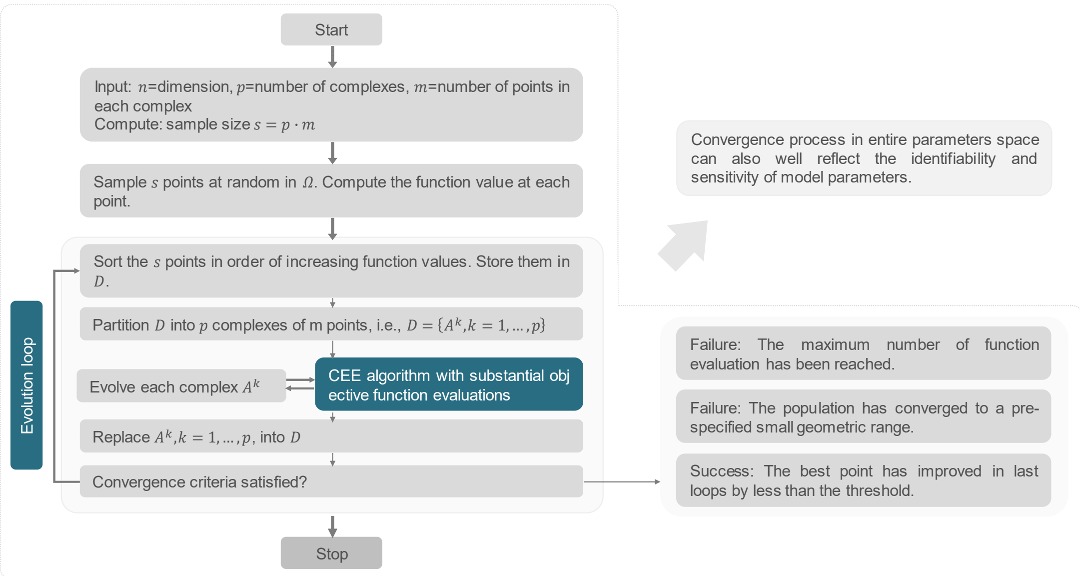

Figure S1. The flowchart of the SCE-UA algorithm (Duan et al., 2010; Duan et al., 1993; Duan et al., 1994).

S2.6 Degree Day Model

The Degree Day Model is a widely used method for estimating the melting of ice and snow. The Degree Day Model is based on a positive linear relationship between glaciers and snowmelt and temperature, especially the positive degree days on the surface of ice and snow. It assumes that when the daily average temperature exceeds the critical temperature for melting, a certain amount of melting occurs. Key parameters include the temperature threshold and the degree day factor (Hock, 2003; Wang et al., 2022).

$$M = \begin{cases} \mathrm{DDF} \cdot \left(T - T_t\right) & T > T_t \\ 0 & T \leq T_t \end{cases} \tag{3}$$

In the formula: is the amount of melt ($mm \cdot d^{-1}$); is the degree day factor ($mm \cdot d^{-1} \cdot °C^{-1}$); is the daily average air temperature (°C); is the critical temperature for melting (°C).

S3 Seasonal dynamic catchment characteristics

S3.1 EDCC algorithmic processes

A systematic approach for Extracting seasonal Dynamic Catchment Characteristics (EDCC) is developed, and the specific procedures are as follows (Fig. S2):

Sampling hydrological processes: The extraction of seasonal dynamic catchment characteristics relies on the computation of relevant indices at the minimum time unit. Therefore, the appropriate sampling of hydrological processes is crucial. It is necessary to avoid excessive discretization or disruption that might impede the normal functioning of hydrological processes while still extracting more detailed and comprehensive information about dynamic catchment characteristics (Choi and Beven, 2007). In light of this, a 15-day moving window serves as the sampling unit, effectively capturing variations in hydrological response resulting from the seasonal dynamics of the catchment. The moving window moves one day at a step with the 14-day overlap between adjacent windows, ensuring the continuity of hydrological processes and facilitating smooth transitions of state variables and fluxes. Each window contains data for the current day and the preceding period, since hydrological processes are responsible for antecedent inputs in the catchment, including meteorology, landscape composition, topography, and other factors (Pande and Moayeri, 2018; Zhang et al., 2018; Li et al., 2015).

Seasonal characteristic index system, consisting of climatic and land-surface subsystems, is designed to systematically capture seasonal dynamic behaviors of catchments, enabling the

EDCC approach to extract valuable information for the enhancement of hydrological model robustness. The index system covers the recent input, memory, and storage dynamics within the catchment system, as detailed in Tables S3-S6 (De Vos et al., 2010a; Peterson et al., 2001; Karl et al., 1999; Guo et al., 2023). The climatic subsystem includes indices for precipitation, temperature, and evapotranspiration. Additionally, extreme climatic indices, referring to the World Climatic Organization Joint Expert Team on Climate Change Detection and Indices, are incorporated into the climate clustering indices, since hydrological behaviours are highly sensitive to them (Tank et al., 2009). Land-surface subsystem comprises the dynamic vegetation cover, antecedent soil moisture, antecedent streamflow, antecedent baseflow, and precipitation-runoff relationships. It is essential to note the difficulty in obtaining monitoring data for land-surface changes, especially in data-limited catchments. Hence, antecedent soil moisture is simulated in advance using hydrological models (De Vos et al., 2010a). As both antecedent streamflow and baseflow are the primary fluxes influencing current runoff at various temporal scales, relevant indices are further taken into consideration (Fan et al., 2017). Moreover, the runoff coefficient, a simple measure reflecting the relationship between precipitation and runoff, is employed in the land-surface subsystem to characterize the catchment's runoff generation capacity (Şen and Altunkaynak, 2006).

Identification of seasonality: The seasonal characteristic index system is designed to provide a comprehensive insight into seasonal dynamic catchment characteristics. However, when applied to a specific basin, not all indices were demonstrated to exhibit significant seasonal dynamics. In response to this, the Seasonality Index (SI) is undertaken to assess the statistical significance of seasonal variations of specific features within the catchment (Swain et al., 2021; Rai and Dimri, 2019), involving SI_{effP}, SI_{T}, SI_{PE}, SI_{NDVI}, and SI_{Q}. Hydrological factors with a seasonality index exceeding 0.6 are deemed to exhibit significant seasonality (Walsh and Lawler, 2012). It is crucial to highlight that the precipitation-runoff relationships, antecedent soil moisture, antecedent streamflow, and antecedent baseflow within the seasonal characteristic index system are directly or indirectly derived from hydrological models or streamflow data. Therefore, the SI_{Q} is employed to depict the seasonality of these indices. The introduction of the seasonality index facilitates an initial screening of indices, ensuring a more targeted and effective posterior screening of indices based on their seasonal characteristics, which enhances the precision of index utilization in specific basins.

Screening of indices: The presence of indices independent of streamflow may potentially disturb the identification of seasonal dynamics in hydrological processes. Therefore, the seasonal characteristic index system is further screened by assessing the degree of complex linear and nonlinear relationships between the indices and streamflow. Maximal Information Coefficient (MIC), as a statistical metric, is employed to indicate both linear and nonlinear correlation between the variables (Zhang et al., 2014). A detailed introduction of the MIC metric is available in the Supporting Information. The screening process utilizes MIC to evaluate the indices. It is assumed that the indices significantly influencing streamflow are screened when the MIC value exceeds 0.35.

Eliminating redundant information: Furthermore, despite the dual screening of indices, a considerable amount of redundant information persists, posing a potential threat to the availability of the extracted information. To mitigate this issue, Principal Components Analysis (PCA) is employed to further eliminate multicollinearity among the indices (Kinney and Atwal, 2014; Maćkiewicz and Ratajczak, 1993).

Clustering hydrological processes: Unsupervised clustering operations are executed based on pre-processed climatic and land-surface index systems. The Fuzzy C-Means (FCM) clustering algorithm was applied for clustering operations (Pathiraja et al., 2018; Bezdek et al., 1984). By employing clustering operations, the calibration period is divided into distinct sub-periods. To mitigate the risk of overfitting associated with an excessive number of sub-periods, it is crucial to predetermine the number of clusters. The elbow technique is employed for this purpose, assessing clustering algorithm performance by cluster validity indices, including the Partition index (*SC*), Separation index (*S*), and Xie and Beni's index (*XB*). These cluster validity indices, commonly used for evaluating the effectiveness of clustering algorithms in data partitioning, contribute to the identification of the optimal number of clusters (Bensaid et al., 1996; Xie and Beni, 1991; De Vos et al., 2010b). Through clustering operations, the hydrological processes are partitioned into distinct sub-periods with similar catchment characteristics.

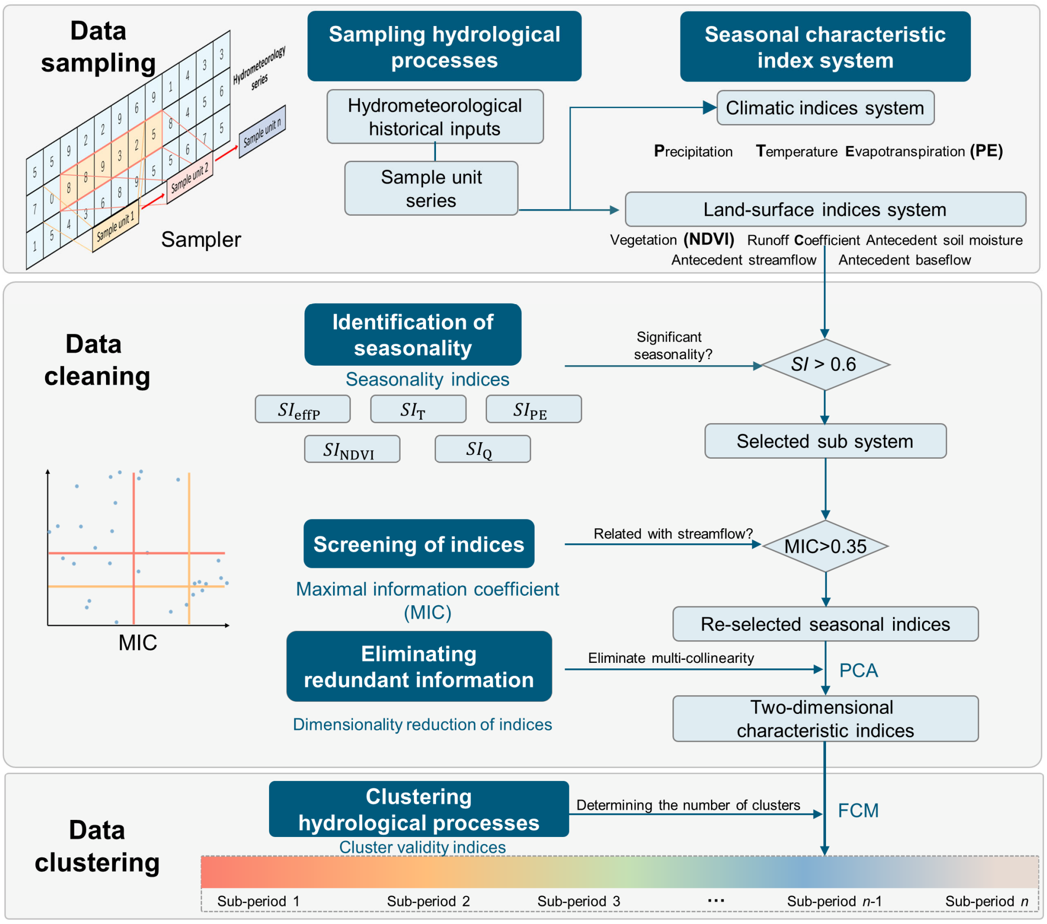

Figure S2. Flowchart illustrating the process of the EDCC approach

Note. In the formula for calculating the Seasonality Index (SI), where R_i represents the annual precipitation, and X_{in} represents the precipitation for month n in a specific i^{th} year. Seasonality indices were computed for effective precipitation (SI_{effP}), temperature (SI_{T}), evaporation (SI_{PE}), NDVI (SI_{NDVI}), and discharge (SI_{Q}). MIC denotes the maximal information coefficient, and PCA stands for principal component analysis.

Table S3. Precipitation indices in climatic index system

Indices	Descriptive names	Definitions	Units	Type	Extreme indices
P	Precipitation	Falling of water from the atmosphere	mm	Recently input	
eff$_P$	Effective precipitation	Precipitation output from the degree day model	mm	Recently input	
P_T	Total precipitation	Total precipitation in window	mm	Memory	
eff$_{PT}$	Total effective precipitation	Total effective precipitation in window	mm	Memory	
RX1day	Maximun 1-day precipitation	Maximun 1 d precipitation in window	mm	Memory	√

RX5day	Maximun 5-day precipitation	Maximun 5 d precipitation in window	mm	Memory	√
R95pTOT	Annual total PRCP when RR > 95p	Total daily precipitation exceeding the 95th percentile of precipitation on wet days	mm	Memory	√
R99pTOT	Annual total PRCP when RR > 99p	Total daily precipitation exceeding the 99th percentile of precipitation on wet days	mm	Memory	√
PRCPTOT	Annual total precipitation in wet days	Total daily precipitation on rainy days	mm	Memory	√
SDII	Simple pricipitation intensity index	Average precipitation on rainy days	mm	Memory	√
R10mm	Annual count of days when PRCP≥ 10mm	Heavy rainfall days: The number of days with daily precipitation (RR) more than 10 mm	days	Memory	√
R20mm	Annual count of days when PRCP≥ 20mm	Heavy rainfall days: The number of days with daily precipitation (RR) more than 20 mm	days	Memory	√
CDD	Maximum length of dry spell	Consecutive drought days: The maximum duration of drought (RR < 1 mm)	days	Memory	√
CWD	Maximum length of wet spell	Consecutive wet days: The maximum duration of wetness (RR > 1 mm)	days	Memory	√

Table S4. Temperature indices in climatic index system

Indices	Descriptive names	Definitions	Units	Type	Extreme indices
T	Temperature	Daily average temperature	°C	Recently input	
T_{max}	Maximum temperature	Daily maximum temperature	°C	Recently input	
T_{min}	Minimum temperature	Daily minimum temperature	°C	Recently input	
$\overline{T}_{max}$	Maximum temperature	Mean daily maximum temperature	°C	Memory	
$\overline{T}_{min}$	Minimum temperature	Mean daily minimum temperature	°C	Memory	
K	Accumulated temperature	The accumulated value of temperatures above 0°C	°C	Memory	
TX_x	Warmest day	The maximum daytime temperature in window	°C	Memory	√
TN_x	Warmest night	The maximum night temperature in window	°C	Memory	√
TX_n	Coldest day	The minimum daytime temperature in window	°C	Memory	√
TN_n	Coldest night	The minimum night temperature in window	°C	Memory	√
FD	Number of frost days	The number of days with T_{min} (daily minimum temperature) < 0°C.	days	Memory	√
SU	Number of summer days	The number of days with T_{max} (daily maximum temperature) > 25°C.	days	Memory	√
ID	Number of icing days	The number of days with T_{max} (daily minimum temperature) < 0°C.	days	Memory	√
TR	Number of tropical nights	The number of days with T_{min} (daily maximum temperature) > 20°C.	days	Memory	√
TN10p	Cold nights	Number of days with T_{min} < 10% (daily maximum temperature series ranked frequency)	days	Memory	√

TX10p	Cold days	Number of days with T_{max} < 10% (daily maximum temperature series ranked frequency)	days	Memory	√
TN90p	Warm nights	Number of days with T_{min} > 90% (daily minimum temperature series ranked frequency)	days	Memory	√
TX90p	Warm days	Number of days with T_{max} > 90% (daily maximum temperature series ranked frequency)	days	Memory	√

Table S5. Evapotranspiration indices in climatic index system

Indices	Descriptive names	Definitions	Units	Type	Extreme indices
PE	Potential evapotranspiration	Evaporation observed from evaporation pan	mm	Recently input	
PE_T	Total potential evapotranspiration	Total pan evaporation in window	mm	Memory	
PE_x	Maximum 1-day potential evapotranspiration	Highest 1 d pan evaporation in window	mm	Memory	
PE_n	Minimum 1-day potential evapotranspiration	Highest 5 d pan evaporation in window	mm	Memory	

Table S6. Vegetation indices in land-surface index system

Indices	Descriptive names	Definitions	Units	Type	Extreme indices
NDVI	Normalized difference vegetation index	The ratio of the difference between near-infrared channel and visible light channel reflectance to their sum.	/	Memory	
C	Runoff coefficient	Ratio of runoff volume to rainfall volume	/	Memory	
$\bar{S}_{t-i}$	Antecedent soil moisture	Antecedent n days soil moisture	/	Storage dynamics	
Q_{t-i}	Antecedent streamflow	Antecedent n days average streamflow	m^3/s	Storage dynamics	
Q_{bt-i}	Antecedent baseflow	Antecedent n days average baseflow	m^3/s	Storage dynamics	

S3.2 Clustering results for EDCC

The results of implementing the EDCC approach in the MOPEX basins are as follows and four selected case studies were analysed in detail. **Identification of seasonality:** The seasonality indices for the MOPEX basins are illustrated in Fig. 1(a). The seasonal dynamics of the MOPEX basins intensify from south to north. Specifically, minimal seasonal variation is observed in the south-eastern basins, while significant seasonality is evident in the central-northern basins, which have been chosen for exploring hydrological models with dynamic catchment characteristics. The seasonality of effective precipitation is predominantly influenced by precipitation, with temperature also playing a noteworthy role, particularly in the central-western and high-latitude mountainous basins. Temperature seasonality becomes more significant with increasing latitude, particularly evident in the Rocky Mountains. Influenced by ocean currents, the west coast exhibits lower temperature seasonality compared to inland regions. The seasonality of potential evapotranspiration, which is positively correlated with temperature, is mainly driven by temperature, which yields geographical patterns that share similarities with temperature patterns, but distinct differences emerge in high-latitude mountainous areas. The northern basins of the Great Plains exhibit the most significant seasonality of NDVI due to the combined effects of precipitation, temperature, and evapotranspiration. Seasonality of antecedent soil moisture simulated by the hydrological model is a holistic response to various inputs and does not exhibit a distinct geographical seasonality. For enhanced clarity in subsequent descriptions, we adopt abbreviations for the four basins mentioned earlier to facilitate in-depth analysis and discussion, which are respectively referred to as Case A (N13302500), Case B (N04073500), Case C (N06192500), and Case D (N08085500). **Screening of indices:** Based on the results of the Seasonality Index (*SI*), the corresponding seasonal characteristic index system was initially screened. To further eliminate interference from the indices with invalid information, complex linear and non-linear relationships between the indices and streamflow are calculated to facilitate the further screening of the index system. The interconnected networks of correlation, as measured by MIC values among all the candidate indices and streamflow in the study cases, are illustrated in Fig. S3. The color depth of the index dots manifests the magnitude of the correlation between the indices and streamflow, while the color of the lines connecting the indices represents the correlation among interconnected indices. There are complex correlations between the indices, ranging from 0.35 to nearly 1 in magnitude, both with streamflow and among the indices themselves. After two-step screening, the number of selected indices in the four study cases is 5, 13, 29, and 12, respectively. **Eliminating redundant information:** The multicollinearity among the screened indices is further addressed before the clustering processes using PCA. The first two principal components (PCs) are selected based on the results of PCA. In the study cases A, B, C, and D, PC1 accounts for 84.0%, 99.5%, 98.0%, and 99.6% of the total variance of indices, respectively. PC2 accounts for 11.6%, 0.3%, 1.5%, and 0.3% of the total variance of indices. These proportions are acceptable (Peres-Neto et al., 2005). **Clustering operations:** In accordance with the cluster validity indices (Fig. 1(c)), the optimal number of clusters for the four study cases has been determined as 5. Fig. 1(d) illustrates the results of the clustering operation. The boundaries of the clusters between different periods are sharp, and the cluster centres exhibit significant spatial dispersion. This clustering outcome is visually represented on the hydrographs in Fig. 1(e). The results suggest that relying solely on climatic indices is insufficient to comprehensively capture the patterns of typical catchment characteristics in hydrological datasets. This inadequacy arises from the fact that hydrological processes influenced by similar climatic patterns can vary significantly due to diverse land-surface influences.

S3.3 MIC values among clustering indices and streamflow

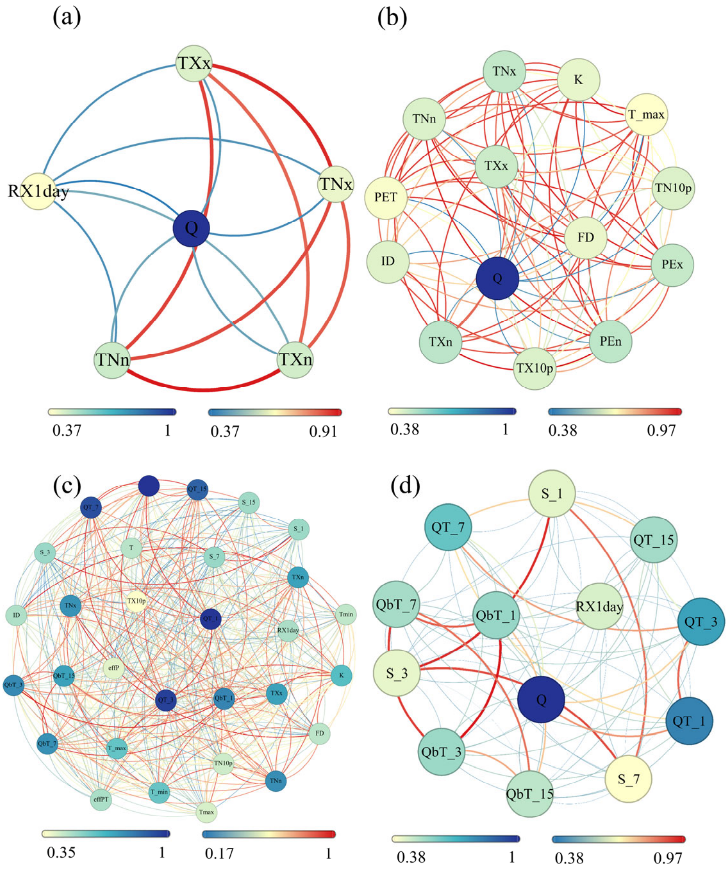

Figure S3. The interconnected network of the nonlinear relationships (MIC values) among the candidate clustering indices and the streamflow in the case A (a), case B (b), case C (c) and case D (d). The nodes correspond to the MIC values between all the candidate inputs and the streamflow. The color of the nodes are proportional to the MIC values. The edges correspond to the MIC values occurring for any two variables (minimum is red; maximum is blue). MIC = maximal information coefficient.

S3.4 Characteristic values in diverse sub-periods in study cases

Table S7. The selected seasonal characteristic indices in diverse sub-periods in case A.

Index	Sub-period 1	Sub-period 2	Sub-period 3	Sub-period 4	Sub-period 5
RX1day	7.18	9.36	11.08	5.83	4.04
TX_x	2.07	9.06	23.38	17.49	27.77
TN_x	-6.31	-2.28	5.79	1.00	8.69
TX_n	-7.97	-0.61	10.01	5.15	18.69

TN_n	-16.10	-12.66	-2.35	-7.63	1.78
Q	0.27	0.31	0.88	0.46	0.42

Table S8. The selected seasonal characteristic indices in diverse sub-periods in case B.

Index	Sub-period 1	Sub-period 2	Sub-period 3	Sub-period 4	Sub-period 5
PE_T	25.31	40.81	15.38	57.86	7.55
PE_x	2.50	3.69	1.61	4.86	0.75
PE_n	1.13	1.91	0.64	2.92	0.32
T_{max}	16.37	22.72	9.11	27.75	-0.52
FD	2.91	0.14	9.84	0.00	14.59
ID	0.01	0.00	0.55	0.00	7.43
TX_x	24.00	28.51	17.75	32.21	6.42
TN_x	10.87	15.77	5.37	19.75	-1.94
TX_n	9.03	16.31	1.63	22.72	-7.69
TN_n	-2.45	3.31	-8.82	9.43	-14.93
TN10p	0.01	0.00	0.31	0.00	4.47
TX10p	0.00	0.00	0.14	0.00	4.55
K	151.68	243.11	63.66	320.50	6.30
Q	1.16	0.91	1.36	0.78	0.88

Table S9. The selected seasonal characteristic indices in diverse sub-periods in case C.

Index	Sub-period 1	Sub-period 2	Sub-period 3	Sub-period 4	Sub-period 5
effP	2.76	4.90	0.99	1.28	0.88
effP$_T$	39.44	87.72	10.75	17.97	10.33
RX1day	9.48	10.02	7.21	7.91	8.42
T	6.68	9.87	-1.93	0.46	-3.02
T_{max}	14.22	18.09	4.57	7.01	3.04
T_{min}	-0.85	1.66	-8.42	-6.08	-9.09
FD	7.62	5.80	13.04	11.38	13.88
ID	1.68	0.00	5.46	4.05	6.40
TX_x	19.50	22.91	10.40	13.42	9.18
TN_x	3.24	4.22	-3.20	-0.85	-3.41
TX_n	7.01	9.70	-2.10	1.15	-4.05
TN_n	-6.03	-2.97	-13.92	-10.78	-14.88
TN10p	0.57	0.00	2.73	1.38	2.84
TX10p	0.80	0.00	2.29	1.60	2.63
K	116.04	132.21	36.08	61.53	27.52
S_1	189.43	222.24	142.26	163.63	89.63
S_3	568.35	667.86	426.32	490.66	267.81
S_7	1326.30	1561.87	993.29	1143.96	620.25
S_{15}	2841.63	3344.28	2127.65	2450.51	1311.95
Q_{T1}	1.23	2.85	0.41	0.56	0.31

Q_{T3}	3.69	8.55	1.21	1.68	0.93
Q_{T7}	8.67	19.92	2.79	3.93	2.16
Q_{T15}	19.06	41.86	5.92	8.55	4.52
Q_{bT1}	0.74	1.36	0.32	0.44	0.24
Q_{bT3}	2.25	4.05	0.96	1.33	0.71
Q_{bT7}	5.33	9.26	2.26	3.13	1.65
Q_{bT15}	11.85	18.83	4.87	6.85	3.51
Q	1.23	2.84	0.41	0.56	0.31

Table S10. The selected seasonal characteristic indices in diverse sub-periods in case D.

Index	Sub-period 1	Sub-period 2	Sub-period 3	Sub-period 4	Sub-period 5
RX1day	16.48	6.37	18.10	10.97	8.94
S_1	138.07	55.04	174.26	114.68	88.14
S_3	414.97	163.94	523.64	343.95	263.96
S_7	967.72	381.99	1221.74	802.11	616.19
Q_{T1}	0.08	0.00	0.29	0.03	0.01
Q_{T3}	0.25	0.01	0.88	0.09	0.04
Q_{T7}	0.59	0.03	2.10	0.21	0.07
Q_{T15}	1.36	0.07	4.23	0.48	0.15
Q_{bT1}	0.02	0.00	0.06	0.01	0.00
Q_{bT3}	0.05	0.01	0.17	0.03	0.01
Q_{bT7}	0.13	0.02	0.38	0.07	0.03
Q_{bT15}	0.28	0.04	0.78	0.14	0.07
Q	0.08	0.01	0.27	0.04	0.02

S4 Test results of the EDCC framework on the MOPEX dataset

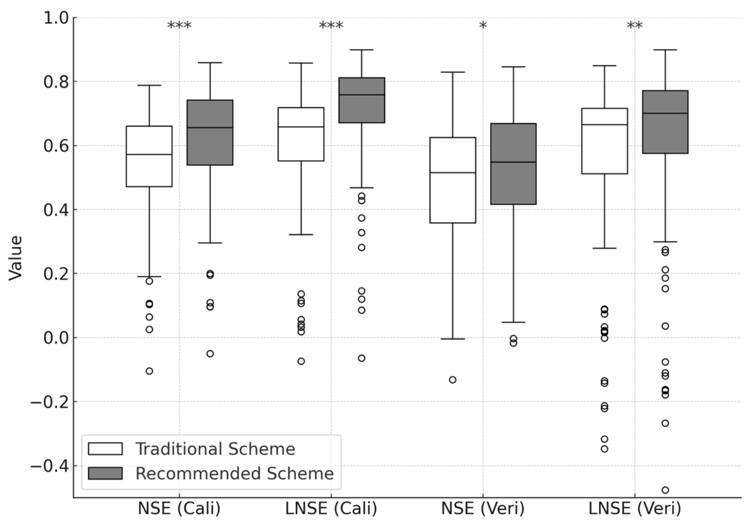

Figure S4. Comparative performance of traditional scheme and recommended scheme on MOPEX dataset across 130 seasonal catchments. Asterisks indicate statistical significance of differences between approaches ($p \leq 0.05$, ** $p \leq 0.01$, *** $p \leq 0.001$).

S5 State variables and fluxes assessment in study cases

The results of state variables and fluxes in case B, C, and D are shown in Fig S5 to Fig S16.

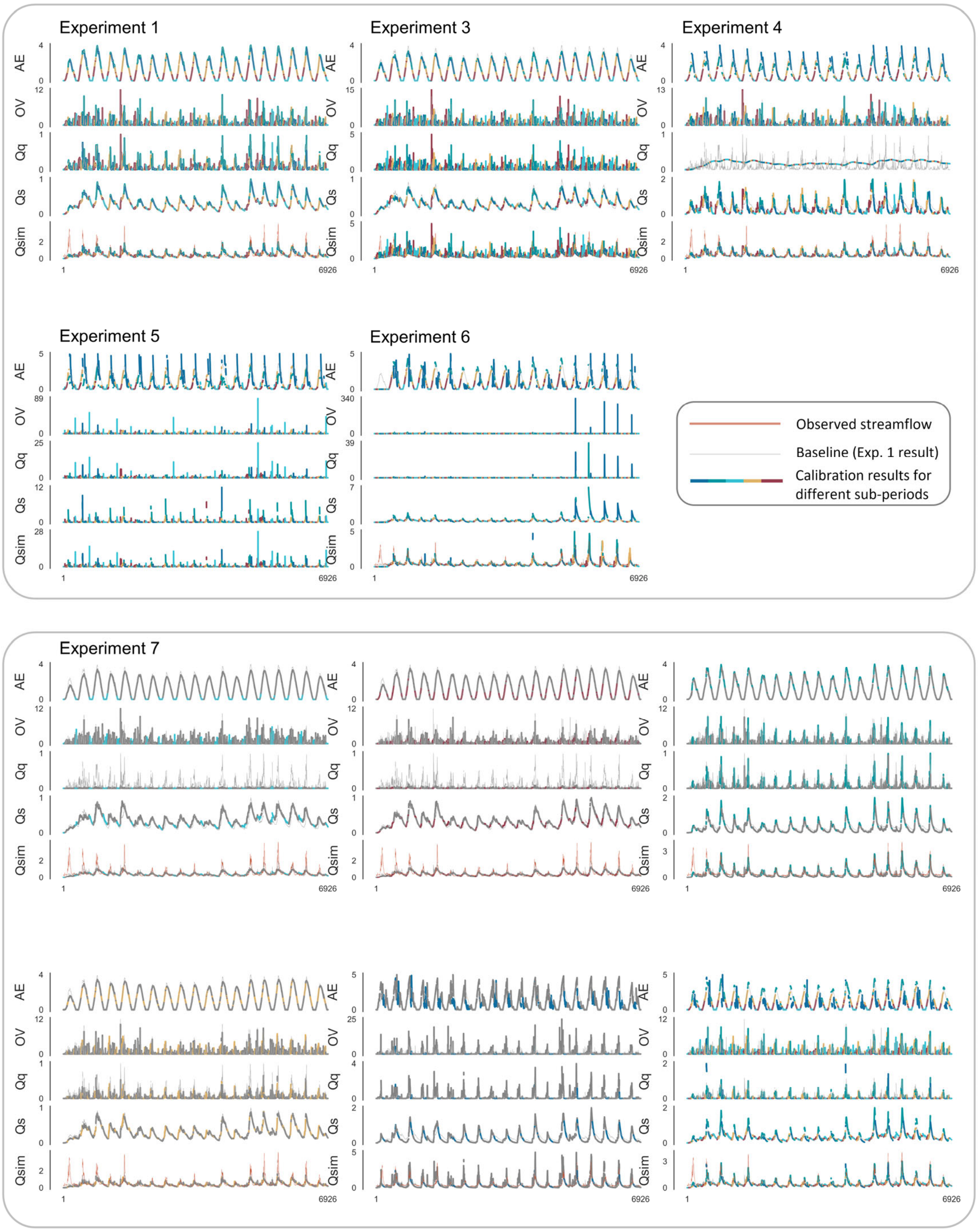

Figure S5. Flux simulation results of experiments over the entire study period for case A. The figure shows the flux simulation results from Experiments 1 to 7, with different colors representing different sub-periods. In Experiment 7, five separate calibrations were performed for five sub-periods, and the results were then aggregated to obtain the final simulation.

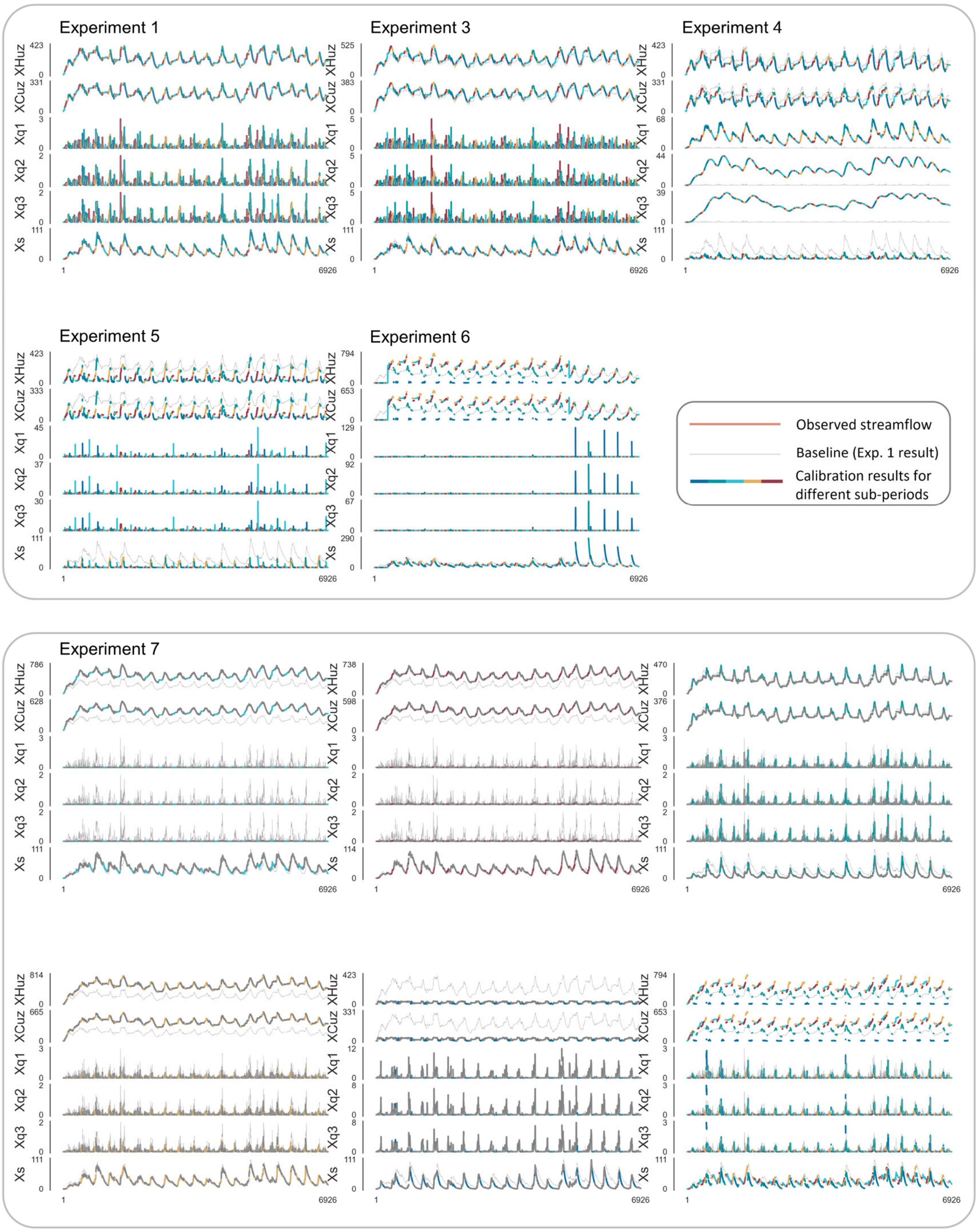

Figure S6. States variables simulation results of experiments over the entire study period for case A. The figure shows the state variable simulation results from Experiments 1 to 7, with different colors representing different sub-periods. In Experiment 7, five separate calibrations were performed for five sub-periods, and the results were then aggregated to obtain the final simulation.

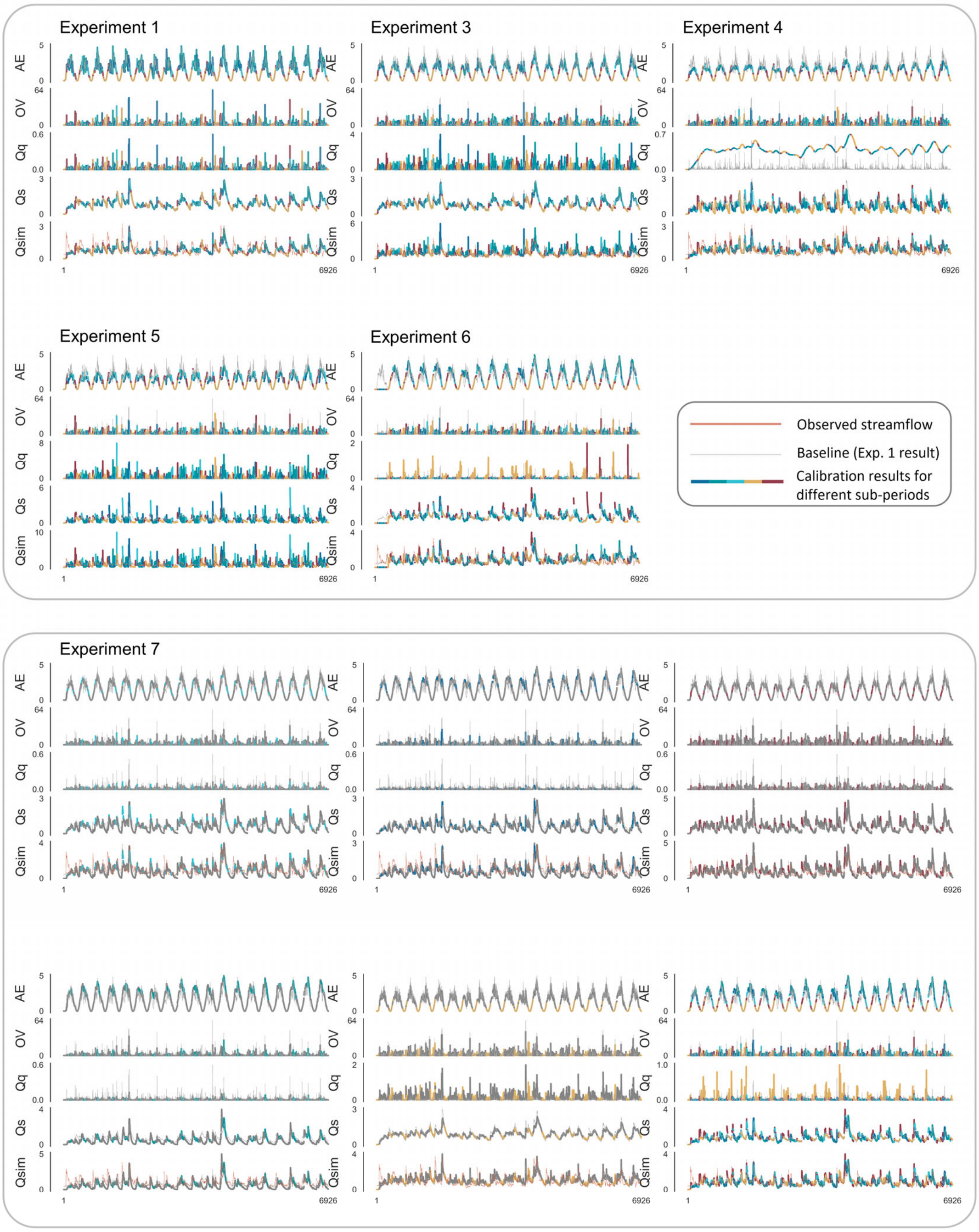

Figure S7. Fluxes simulation results of experiments over the entire study period for case B.

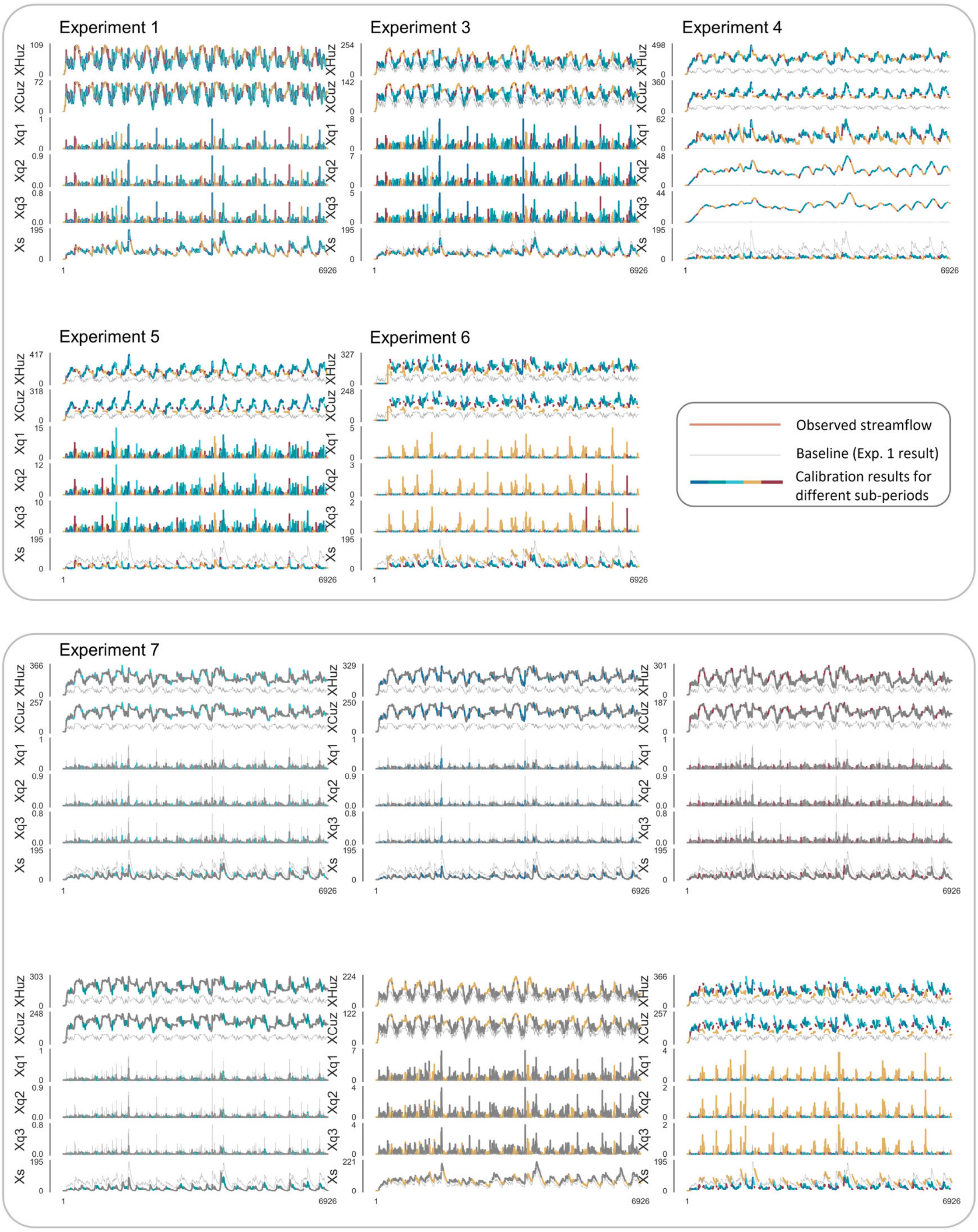

Figure S8. States variables simulation results of experiments over the entire study period for case B.

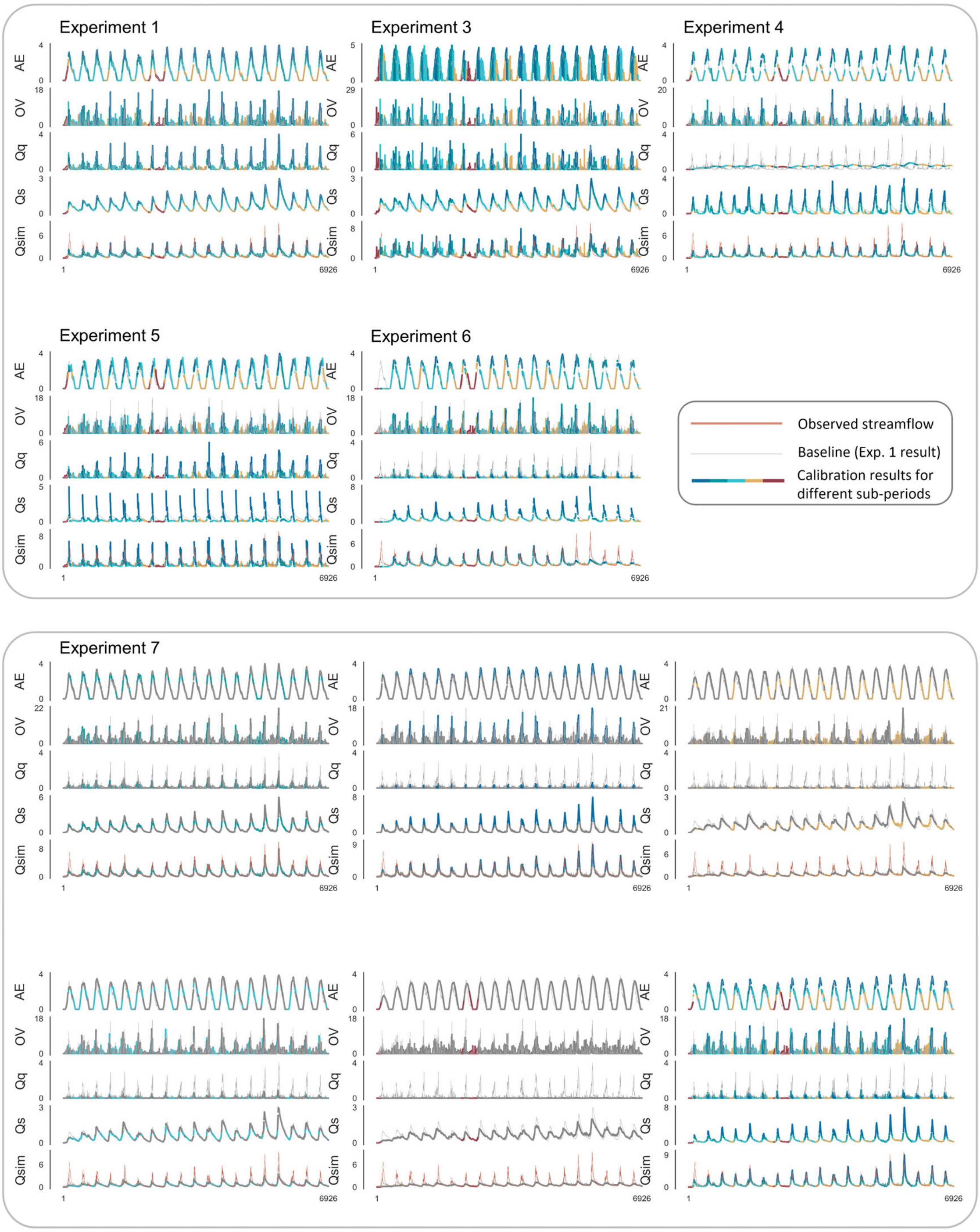

Figure S9. Fluxes simulation results of experiments over the entire study period for case C.

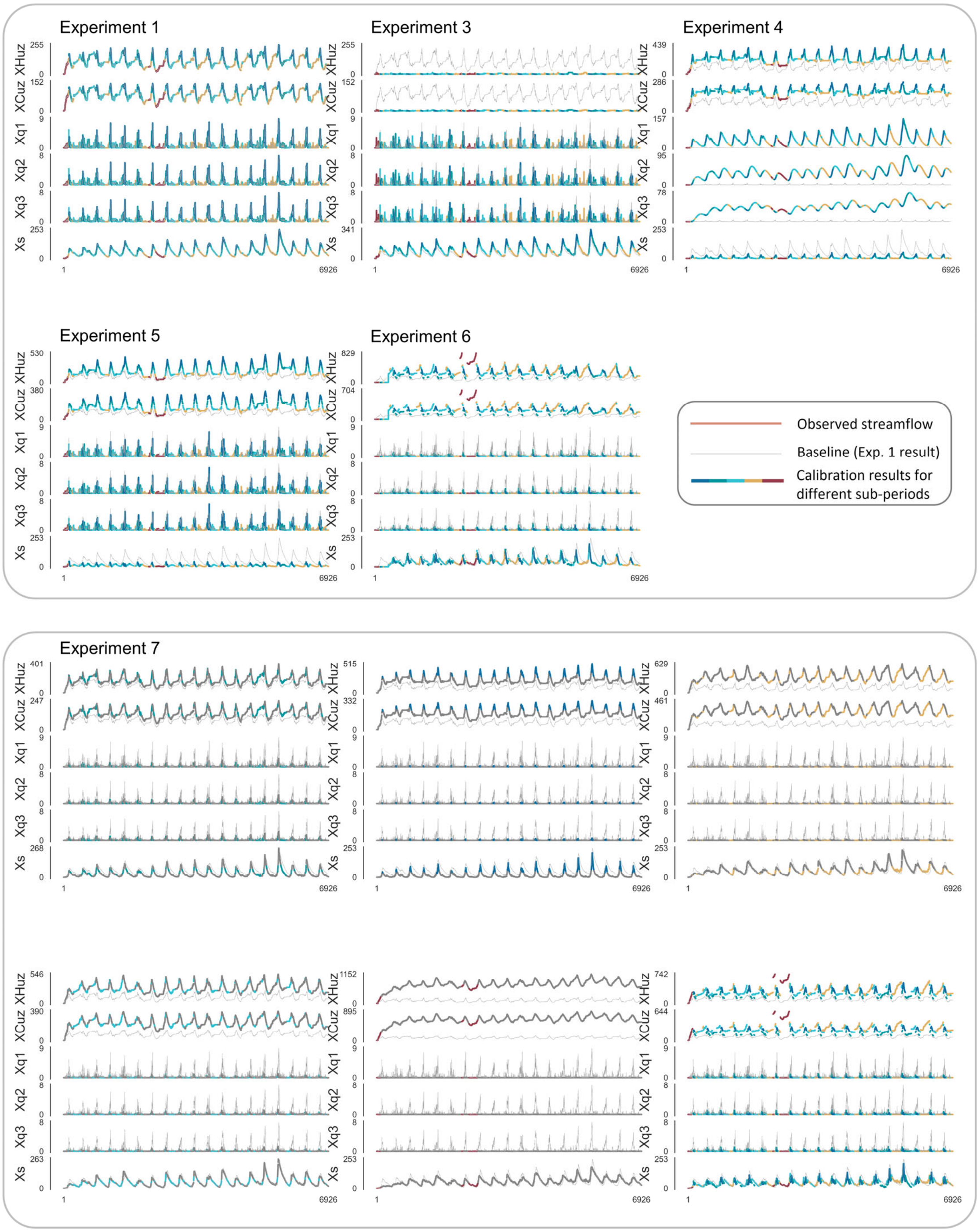

Figure S10. States variables simulation results of experiments over the entire study period for case C.

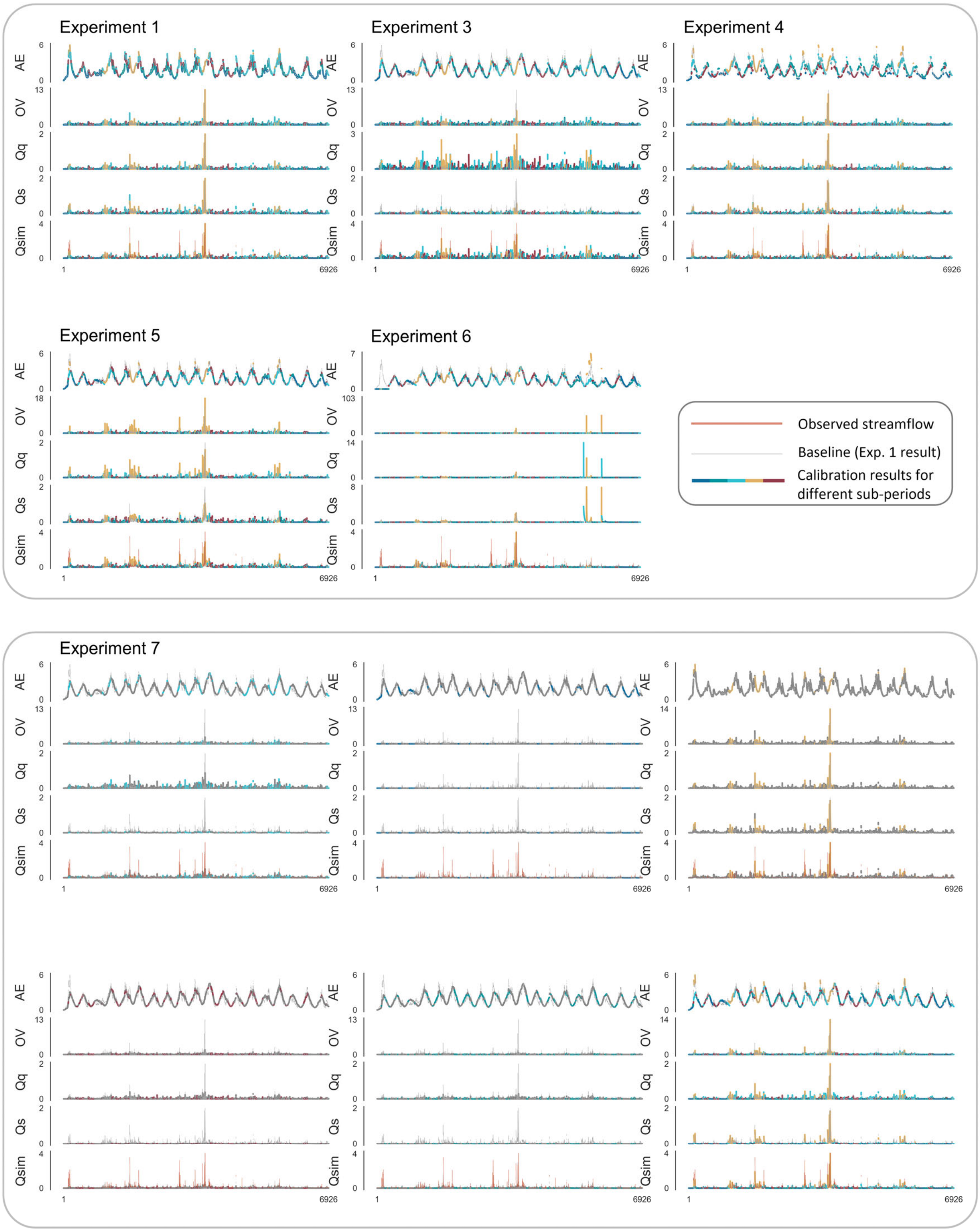

Figure S11. Fluxes simulation results of experiments over the entire study period for case D.

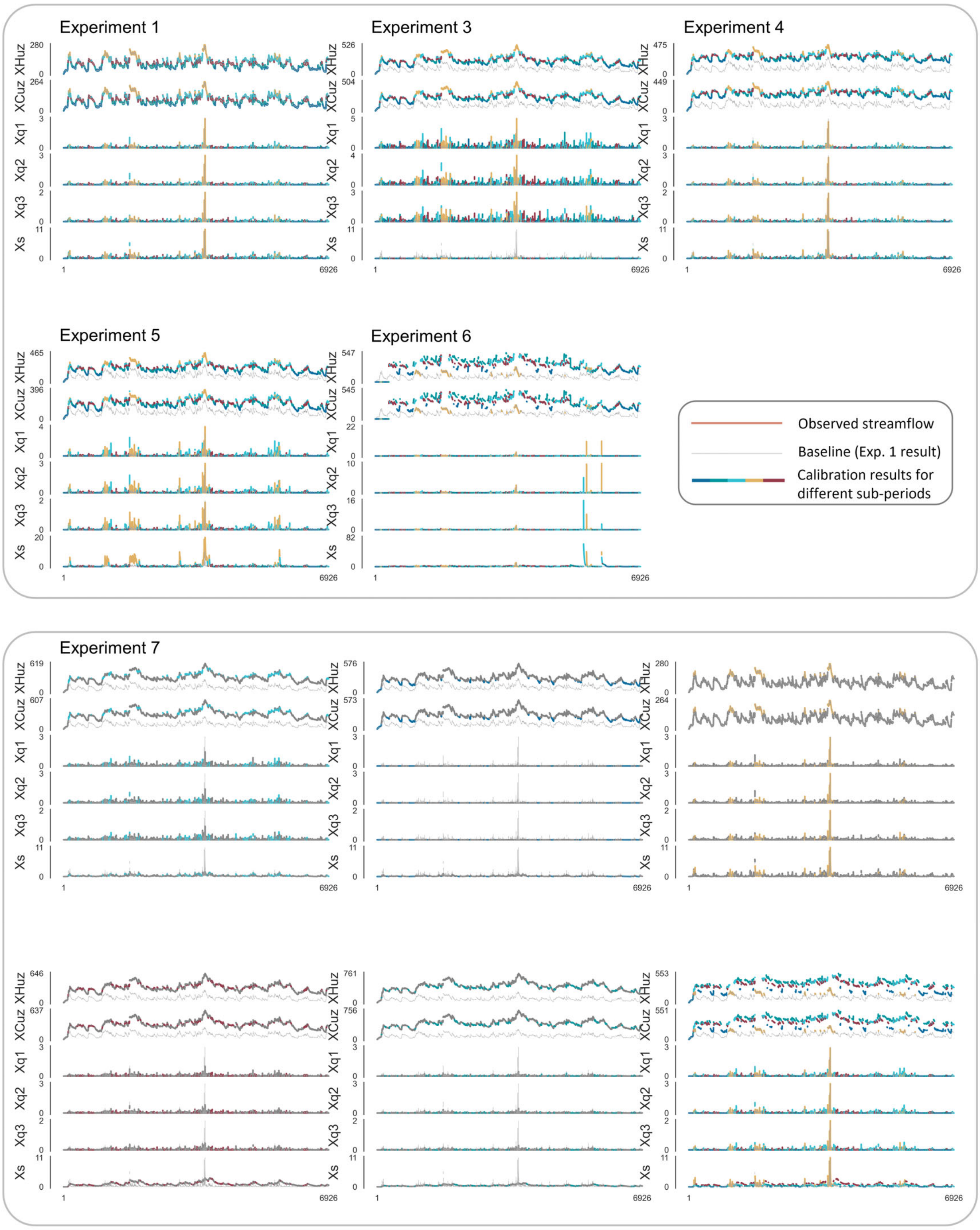

Figure S12. States variables simulation results of experiments over the entire study period for case D.

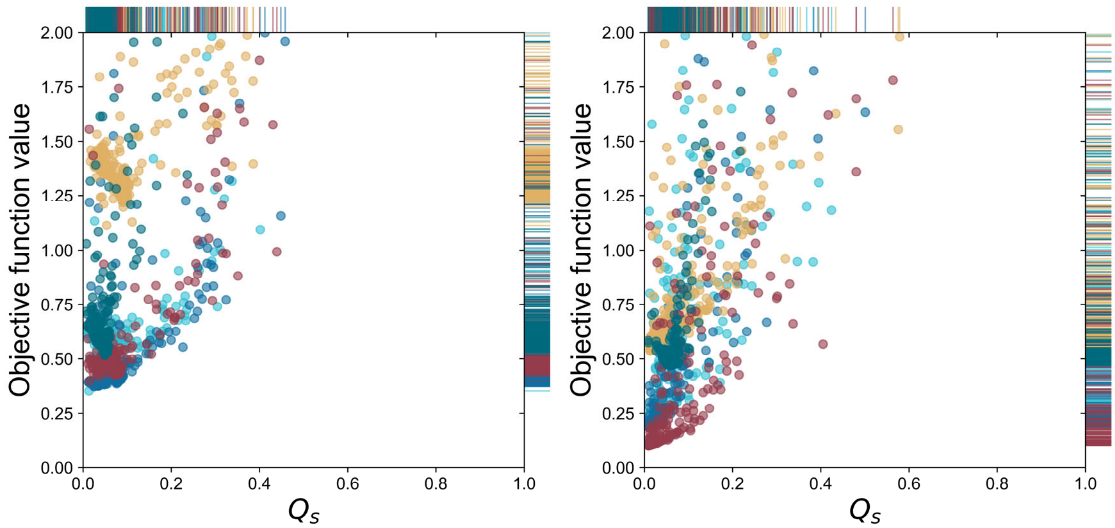

Figure S13. Flux mapping of study case B. The left image is the traditional scheme, the right image represents the recommended scheme.

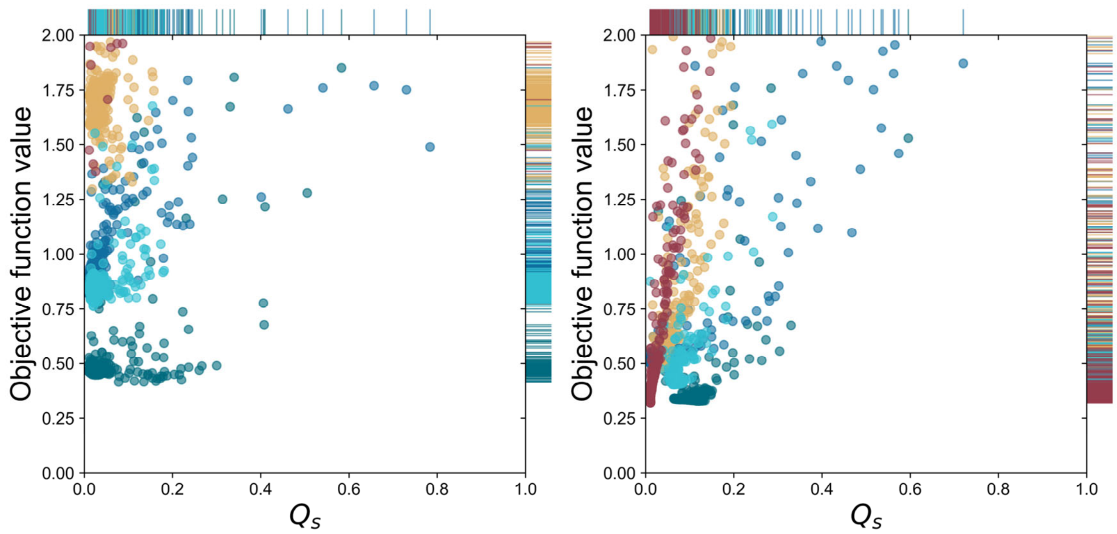

Figure S14. Flux mapping of study case C. The left image is the traditional scheme, the right image represents the recommended scheme.

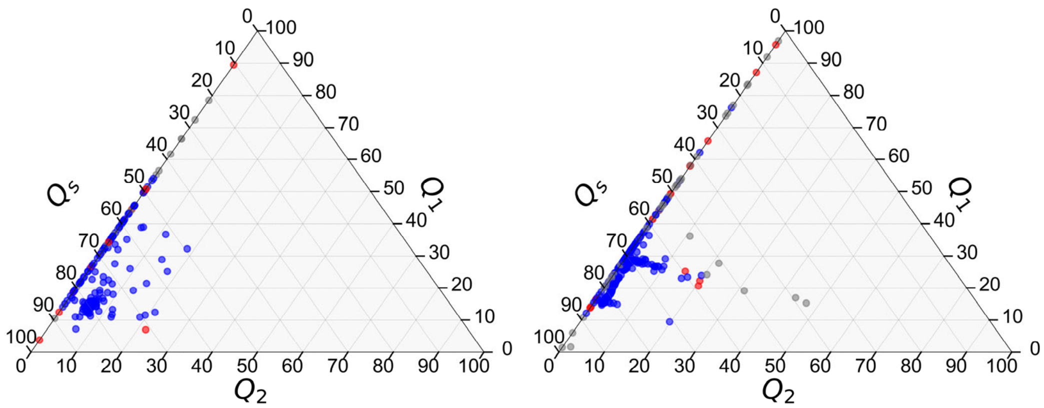

Figure S15. Flux mapping of study case C period 3. The left image is the traditional scheme, the right image represents the recommended scheme.

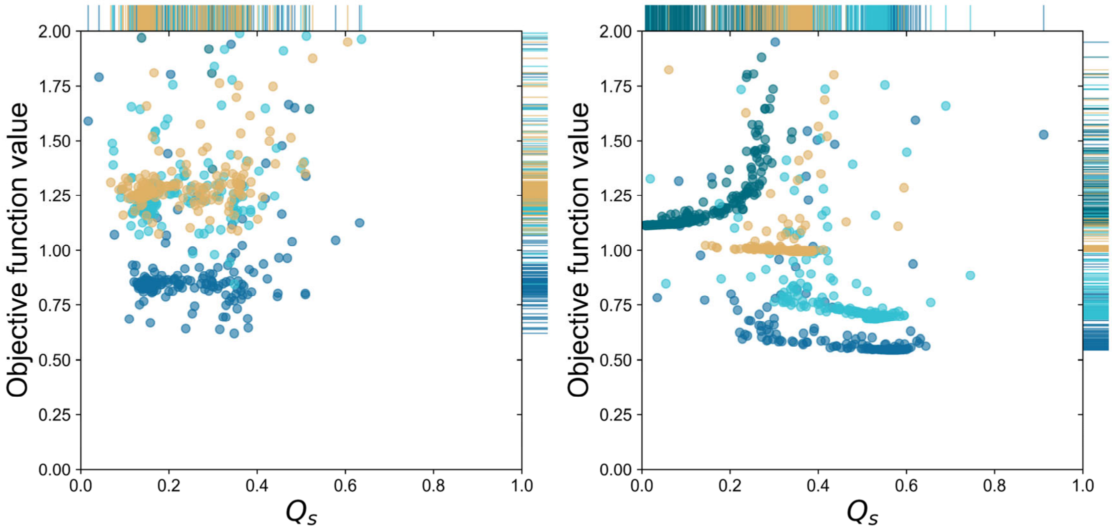

Figure S16. Flux mapping of study case D. The left image is the traditional scheme, the right image represents the recommended scheme.

S6 Correlation between model parameters

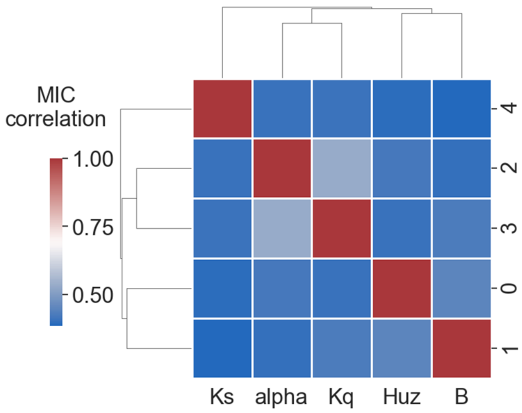

Figure S17. Correlation between model parameters in study case B.

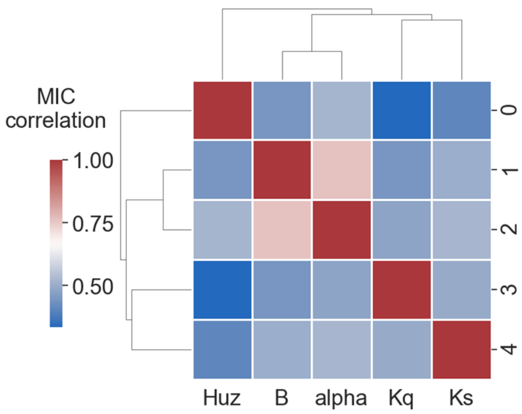

Figure S18. Correlation between model parameters in study case C.

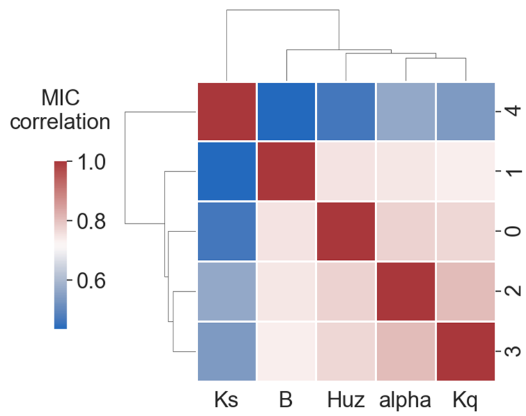

Figure S19. Correlation between model parameters in study case D.

References

Bensaid, A. M., Hall, L. O., Bezdek, J. C., Clarke, L. P., Silbiger, M. L., Arrington, J. A., and Murtagh, R. F.: Validity-guided (re)clustering with applications to image segmentation, IEEE Transactions on Fuzzy Systems, 4, 112-123, 10.1109/91.493905, 1996.

Bezdek, J. C., Ehrlich, R., and Full, W.: FCM: The fuzzy c-means clustering algorithm, Computers & Geosciences, 10, 191-203, 10.1016/0098-3004(84)90020-7, 1984.

Cheng, L., Yaeger, M., Viglione, A., Coopersmith, E., Ye, S., and Sivapalan, M.: Exploring the physical controls of regional patterns of flow duration curves – Part 1: Insights from statistical analyses, Hydrology and Earth System Sciences, 16, 4435-4446, 10.5194/hess-16-4435-2012, 2012.

Choi, H. T. and Beven, K.: Multi-period and multi-criteria model conditioning to reduce prediction uncertainty in an application of TOPMODEL within the GLUE framework, Journal of Hydrology, 332, 316-336, 10.1016/j.jhydrol.2006.07.012, 2007.

De Vos, N., Rientjes, T., and Gupta, H.: Diagnostic evaluation of conceptual rainfall–runoff models using temporal clustering, Hydrological Processes, 24, 2840-2850, 2010a.

de Vos, N. J., Rientjes, T. H. M., and Gupta, H. V.: Diagnostic evaluation of conceptual rainfall–runoff models using temporal clustering, Hydrological Processes, 24, 2840-2850, 10.1002/hyp.7698, 2010b.

Duan, Q., Sorooshian, S., and Gupta, V.: Effective and efficient global optimization for conceptual rainfall-runoff models, Water Resour Res, 28, 1015-1031, 10.1029/91wr02985, 2010.

Duan, Q. Y., Gupta, V. K., and Sorooshian, S.: Shuffled Complex Evolution Approach for Effective and Efficient Global Minimization, Journal of Optimization Theory and Applications, 76, 501-521, Doi 10.1007/Bf00939380, 1993.

Duan, Q. Y., Sorooshian, S., and Gupta, V. K.: Optimal use of the SCE-UA global optimization method for calibrating watershed models, Journal of Hydrology, 158, 265-284, doi.org/10.1016/0022-1694(94)90057-4 1994.

Dunn, J. C.: A fuzzy relative of the ISODATA process and its use in detecting compact well-separated clusters, Journal of Cybernetics 3(3), 32–57, 10.1080/01969727308546046, 1973.

Eckhardt, K. and Arnold, J. G.: Automatic calibration of a distributed catchment model, Journal of Hydrology, 251, 103-109, 10.1016/s0022-1694(01)00429-2, 2001.

Fan, Y. R., Huang, G. H., Li, Y. P., Wang, X. Q., Li, Z., and Jin, L.: Development of PCA-based cluster quantile regression (PCA-CQR) framework for streamflow prediction: Application to the Xiangxi river watershed, China, Applied Soft Computing, 51, 280-293, 10.1016/j.asoc.2016.11.039, 2017.

Frey, D. and Pimentel, R.: Principal component analysis and factor analysis, 1978.

Ghumman, A. R., Jamaan, M., Ahmad, A., Shafiquzzaman, M., Haider, H., Al Salamah, I. S., and Ghazaw, Y. M.: Simulation of pan-evaporation using penman and hamon equations and artificial intelligence techniques, Water, 13, 793, 10.3390/w13060793, 2021.

Guo, J., Liang, X., Wang, X., Fan, Y., and Liu, L.: Potential benefits of limiting global warming for the mitigation of temperature extremes in China, npj Climate and Atmospheric Science, 6, 106, 10.1038/s41612-023-00412-4, 2023.

Gupta, H. V., Kling, H., Yilmaz, K. K., and Martinez, G. F.: Decomposition of the mean squared error and NSE performance criteria: Implications for improving hydrological modelling, Journal of Hydrology, 377, 80-91, 10.1016/j.jhydrol.2009.08.003, 2009.

Hamon, W. R.: Estimating potential evapotranspiration, Journal of the Hydraulics Division, 87, 107-120, 10.1061/jyceaj.0000599, 1961.

Hathaway, R. J. and Bezdek, J. C.: Fuzzy c-means clustering of incomplete data, IEEE Transactions on Systems, Man, and Cybernetics, Part B (Cybernetics), 31, 735-744, 10.1109/3477.956035, 2001.

Hock, R.: Temperature index melt modelling in mountain areas, Journal of Hydrology, 282, 104-115, 10.1016/s0022-1694(03)00257-9, 2003.

Karl, T. R., Nicholls, N., and Ghazi, A.: Clivar/GCOS/WMO workshop on indices and indicators for climate extremes workshop summary, Weather and climate extremes: Changes, variations and a perspective from the insurance industry, 3-7, doi.org/10.1007/978-94-015-9265-9_2, 1999.

Khakbaz, F. and Kazeminezhad, M.: Work hardening and mechanical properties of severely deformed AA3003 by constrained groove pressing, Journal of Manufacturing Processes, 14, 20-25, 10.1016/j.jmapro.2011.07.001, 2012.

Kinney, J. B. and Atwal, G. S.: Equitability, mutual information, and the maximal information coefficient, Proceedings of the National Academy of Sciences, 111, 3354-3359, 10.1073/pnas.1309933111, 2014.

Li, S., Xiong, L., Li, H.-Y., Leung, L. R., and Demissie, Y.: Attributing runoff changes to climate variability and human activities: uncertainty analysis using four monthly water balance models, Stoch Env Res Risk A, 30, 251-269, 10.1007/s00477-015-1083-8, 2015.

Maćkiewicz, A. and Ratajczak, W.: Principal components analysis (PCA), Computers & Geosciences, 19, 303-342, 1993.

McCabe, G. J., Hay, L. E., Bock, A., Markstrom, S. L., and Atkinson, R. D.: Inter-annual and spatial variability of Hamon potential evapotranspiration model coefficients, Journal of Hydrology, 521, 389-394, 10.1016/j.jhydrol.2014.12.006, 2015.

Morton, F. I.: Catchment evaporation and potential evaporation further development of a climatologic relationship, Journal of Hydrology, 12, 81-99, 10.1016/0022-1694(71)90102-8, 1971.

Pande, S. and Moayeri, M.: Hydrological Interpretation of a Statistical Measure of Basin Complexity, Water Resour Res, 54, 7403-7416, 10.1029/2018wr022675, 2018.

Pathiraja, S., Anghileri, D., Burlando, P., Sharma, A., Marshall, L., and Moradkhani, H.: Time-varying parameter models for catchments with land use change: the importance of model structure, Hydrol Earth Syst Sc, 22, 2903-2919, 10.5194/hess-22-2903-2018, 2018.

Peres-Neto, P. R., Jackson, D. A., and Somers, K. M.: How many principal components? stopping rules for determining the number of non-trivial axes revisited, Computational Statistics & Data Analysis, 49, 974-997, 10.1016/j.csda.2004.06.015, 2005.
Peterson, T., Folland, C., Gruza, G., Hogg, W., Mokssit, A., and Plummer, N.: Report on the activities of the working group on climate change detection and related rapporteurs, World Meteorological Organization Geneva2001.
Pfannerstill, M., Guse, B., and Fohrer, N.: Smart low flow signature metrics for an improved overall performance evaluation of hydrological models, Journal of Hydrology, 510, 447-458, 10.1016/j.jhydrol.2013.12.044, 2014.
Rai, P. and Dimri, A. P.: Changes in rainfall seasonality pattern over India, Meteorological Applications, 27, e1823, 10.1002/met.1823, 2019.
Reshef, D. N., Reshef, Y. A., Finucane, H. K., Grossman, S. R., McVean, G., Turnbaugh, P. J., Lander, E. S., Mitzenmacher, M., and Sabeti, P. C.: Detecting novel associations in large data sets, Science, 334, 1518-1524, 10.1126/science.1205438, 2011.
Şen, Z. and Altunkaynak, A.: A comparative fuzzy logic approach to runoff coefficient and runoff estimation, Hydrological Processes, 20, 1993-2009, 10.1002/hyp.5992, 2006.
Sorooshian, S., Duan, Q., and Gupta, V. K.: Calibration of rainfall-runoff models: Application of global optimization to the Sacramento Soil Moisture Accounting Model, Water Resour Res, 29, 1185-1194, 10.1029/92wr02617, 2010.
Swain, S., Mishra, S. K., Pandey, A., and Dayal, D.: Spatiotemporal assessment of precipitation variability, seasonality, and extreme characteristics over a Himalayan catchment, Theoretical and Applied Climatology, 147, 817-833, 10.1007/s00704-021-03861-0, 2021.
Vrugt, J. A., Gupta, H. V., Bouten, W., and Sorooshian, S.: A Shuffled Complex Evolution Metropolis algorithm for optimization and uncertainty assessment of hydrologic model parameters, Water Resour Res, 39, 10.1029/2002wr001642, 2003.
Wagener, T., Boyle, D. P., Lees, M. J., Wheater, H. S., Gupta, H. V., and Sorooshian, S.: A framework for development and application of hydrological models, Hydrology and Earth System Sciences, 5, 13-26, 10.5194/hess-5-13-2001, 2001.
Walsh, R. P. D. and Lawler, D. M.: Rainfall Seasonality: Description, Spatial Patterns and Change through Time, Weather, 36, 201-208, 10.1002/j.1477-8696.1981.tb05400.x, 2012.
Wang, Y., Wang, J., Xie, J., and Lu, H.: Improvements in the degree-day model, incorporating forest influence, and taking China's Tianshan Mountains as an example, Journal of Hydrology: Regional Studies, 44, 10.1016/j.ejrh.2022.101215, 2022.
Wold, S., Esbensen, K., and Geladi, P.: Principal component analysis, Chemometrics and intelligent laboratory systems, 2, 37-52, 10.1016/0169-7439(87)80084-9, 1987.
Wright, J., Ganesh, A., Rao, S., Peng, Y., and Ma, Y.: Robust principal component analysis: Exact recovery of corrupted low-rank matrices via convex optimization, Advances in neural information processing systems, 22, 2009.
Xie, X. L. and Beni, G.: A validity measure for fuzzy clustering, IEEE Transactions on Pattern Analysis and Machine Intelligence, 13, 841-847, 10.1109/34.85677, 1991.
Zhang, Y., Jia, S., Huang, H., Qiu, J., and Zhou, C.: A Novel Algorithm for the Precise Calculation of the Maximal Information Coefficient, Scientific Reports, 4, 6662, 10.1038/srep06662, 2014.
Zhang, Y., Liu, S., Hou, X., Cheng, F., and Shen, Z.: Landscape- and climate change-induced hydrological alterations in the typically urbanized Beiyun River basin, Beijing, China, Stoch Env Res Risk A, 33, 149-168, 10.1007/s00477-018-1628-8, 2018.